Analyst

ROYAL SOCIETY OF CHEMISTRY

PAPER

View Article Online
View Journal | View Issue

Cite this: *Analyst*, 2026, **151**, 2049

A direct comparison of antibody and nanoMIP binding affinities to a protein target using surface plasmon resonance and electrochemical techniques: a haemoglobin model

Andrei N. Stephen, † Barbara V. Boldrin† and Subrayal M. Reddy *

This study presents, for the first time, a direct quantitative comparison between the binding affinities and selectivities of antibodies and their molecularly imprinted polymer (nanoMIP) counterparts for a target protein antigen. NanoMIPs were synthesized upon protein functionalised magnetic nanoparticles (MNPs) using bovine haemoglobin as a target protein. This solid-phase synthesis process gave nanoMIP yields of 10 ± 2 mg produced in less than 1 h. Physical characterization of nanoMIPs by dynamic light scattering (DLS) revealed an average particle diameter of 121 ± 53 nm, consistent with nanoparticle tracking analysis (NTA) results, confirming uniform particle formation and comparable concentrations to antibody preparations. Antibody and nanoMIP affinities were characterized using surface plasmon resonance (SPR), the current gold-standard technique, as well as using a newly developed electrochemical method based on electrochemical impedance spectroscopy (EIS). This dual approach enables direct comparison and standardization of nanoMIPs as synthetic alternatives to conventional antibodies. NanoMIP binding affinities of 34.7 ± 2 pM (EIS) and 3.06 pM (SPR) were obtained, with a selectivity factor of 130 : 1 (target : non-target) based on the electrochemical method. In contrast, the corresponding polyclonal antibody for haemoglobin (pAb) demonstrated contrasting affinities of 51.9 ± 0.74 pM (EIS) and 48.7 nM (SPR) and with a substantially lower selectivity factor of 1 : 1.1. These results indicate that while the two sensor techniques are ideal for nanoMIP characterisation, further harmonisation is required for antibody binding characterisation. We demonstrate that the developed nanoMIPs not only rival but can surpass traditional animal-derived antibodies in both affinity and molecular discrimination. Overall, these findings highlight nanoMIPs as a robust and reproducible alternative to antibodies, offering superior selectivity and comparable affinity for next-generation bioanalytical and diagnostic applications.

Received 14th November 2025,
Accepted 22nd January 2026

DOI: 10.1039/d5an01205h

rsc.li/analyst

Introduction

Animal-derived antibodies are heavily used in the biomedical field for research, diagnostic and therapeutic purposes given their molecular recognition capability and high selectivity and affinity.[1] Despite being a well-established technology, the use of monoclonal and polyclonal antibodies does not come without drawbacks. They have a narrow stability range of temperature and pH, can take months to produce, and rely on animal immunisation, culminating in high cost that can vary from $10 to $100 per gram[2] (at the time of writing this paper). Moreover, concerns with batch-to-batch variability, especially in the case of polyclonal antibodies,[3] have contributed to the need for replacement alternatives, and have even been strongly emphasized by regulatory agencies, healthcare authorities[4] and the EU directive 2010/63/EU.[5] To this end, molecularly imprinted polymers (MIPs) have gained traction over the past 25 years due to their antibody-like affinity and selectivity towards target molecules, stability, low cost and speed of production,[6,7] becoming the most studied biomimetic material.[8]

MIPs are synthetic affinity reagents produced typically by the self-assembly of functional monomers around a template, for example, a protein[9] or virus,[10] driven mostly by hydrogen bonding but also by van der Waals forces and π–π interactions. In the presence of initiators and a cross-linker, a polymeric matrix is formed surrounding the template.[11] When removed, the template leaves behind cavities (binding sites) complementary in size and shape, capable of selective recognition of the target. Acrylamide-based polymer hydrogels have been widely researched, producing MIPs capable of protein recognition.[12]

Centre for Smart Materials, University of Lancashire, Preston, PR1 2HE, UK.
E-mail: smreddy@lancashire.ac.uk
† These two authors contributed equally to this work.

They can be rapidly produced in large (mg to gram) quantities using inexpensive reagents in less than a day in a one-pot synthesis, as demonstrated by our recent work.[6]

Historically, MIP synthesis consisted of a top-down approach forming a polymeric hydrogel monolith (bulk) using acryloyl-based monomers such as acrylamide, acrylic acid and *N*-hydroxymethylacrylamide (NHMA). The hydrogel monolith was further broken down by sieving or grinding, producing micron-sized particles exposing target-specific cavities on each particle surface.[13,14] In addition to being a laborious process and demanding large amounts of template protein, the rudimentary nature of bulk MIP production resulted in limited control over physical characteristics such as particle size and cavity density, leading to the production of random nanoscale features in addition to the desired binding sites. MIPs produced in this way therefore have little homogeneity and are prone to non-specific binding, resulting in lower binding affinities for the target. Recent methods have focused on forming nanoscale MIPs (nanoMIPs), making use of a bottom-up approach to form MIP particles with similar dimensions to the target, resulting in higher affinity as binding sites are one-to-one with the target protein. Two approaches have been explored to obtain these high affinity nanoMIPs: solid-phase[6,15] and solution-phase.[7,16,17] However, the integration of nanoMIPs obtained by either method into conventional surface plasmon resonance (SPR) sensing platforms does not reflect their high affinities. The immobilization of nanoMIPs onto SPR sensor surfaces requires chemical modification, for example, by a coupling procedure using 1-ethyl-3-(3-dimethylaminopropyl) carbodiimide (EDC) and *N*-hydroxysuccinimide (NHS),[18] constituting a significant challenge and also increasing the time and cost of the process.

As an alternative, MIPs can be electrochemically synthesized directly on the surface of screen-printed electrodes, where a polymeric hydrogel thin-film layer is formed (E-MIPs),[9,10,12] making use of a monomer solution containing the target template. After removal of the target, the resulting cavities are exposed on the surface of the thin film, and rebinding can be detected by electrochemical (EC) methods such as electrochemical impedance spectroscopy (EIS). E-MIPs have been demonstrated to be a straightforward, cheap and versatile biosensing method for detecting biomarkers. Combining the high affinity of nanoMIPs with the simplicity of electrosynthesized E-MIPs, our group recently developed a sensing platform by physically entrapping nanoMIPs into an electropolymerized thin-film layer (E-layer) on the surface of a screen-printed electrode (SPE) using cyclic voltammetry (CV).[6,7] Advantages of the developed system include fine control over layer deposition,[9] inherent polymeric compatibility between nanoMIPs and the E-layer facilitating seamless integration, and there is no requirement for chemical coupling reagents or blocking steps.

The application of MIPs to biosensing has been explored using different techniques including using a quartz crystal microbalance (QCM),[9,19,20] and using electrochemical[9,10,12,21,22] and optical sensors[7,23–25] with a focus on real-life and point-of-care applications.[26,27] SPR has emerged as the gold standard technique for the investigation of interactions between antibody and antigens and the detection of biomarkers.[28] The characterization of nanoMIPs using surface plasmon resonance (SPR) has gained attention as a comparative tool to antibodies. The technology is based on the optical phenomenon occurring when polarized light interacts with a metal layer (*e.g.* gold) that is deposited on a prism with a high refractive index. When the light is at a critical angle of incidence, the energy is transferred to the metal electrons, generating a surface plasmon. Changes on the metal surface, for example, the adsorption of biomolecules and antibody–antigen interaction, cause variation in the refractive light intensity and angle of reflection, allowing real-time characterization of binding and unbinding events with high sensitivity.[29] The kinetics of the interaction is expressed in terms of affinity (K_D), association (k_{on}) and dissociation (k_{off}) constants. Although SPR has been applied to characterize both MIPs and antibodies, they are essentially distinct biomaterials, one being synthetic and the other being biological in nature, with differences in size, structure and orientation of the binding sites. Such characteristics are key for a critical step of sensing by SPR – the immobilization of the ligand (antibody or nanoMIP) onto the surface of a sensor chip (usually made of gold), commonly by covalent and irreversible amine coupling *via* EDC/NHS chemistry.[29] Another factor is the imprinting method for producing MIPs, where the entire template (protein) is used, likely leaving behind, after its removal, cavities that are complementary to multiple binding sites found at the surface of the protein structure, contrasting to the specific epitope region available for antigen binding on antibodies (Fab: fragment antigen-binding). Additionally, the penetration depth of commonly used SPR chips is approximately 216 nm.[24] Antibodies have an average hydrodynamic diameter of 9–12 nm[30] while nanoMIP sizes range from 50 to 200 nm.[7] As a result, interactions with materials that approximate or exceed the penetration depth are unable to generate detectable results, limiting the applicability of SPR to nanoMIPs.

To date, there has been no direct comparison between nanoMIPs and antibodies using SPR. Such an approach enables the evaluation of binding kinetics and affinities under identical experimental conditions, providing a more rigorous assessment of their relative performance. While previous comparisons have been made using techniques such as ELISA,[31,32] these methods offer only limited insights into the nature of molecular interactions. In contrast, SPR provides real-time monitoring of binding events, allowing for a detailed analysis of association and dissociation processes. This makes SPR particularly well-suited to determining whether nanoMIPs and antibodies differ in how they recognise and interact with their target molecules. In this paper, we use an in-house developed EC method for characterising nanoMIPs[6,7,33] in addition to the gold standard SPR method to obtain affinity and selectivity results for both antibodies and nanoMIPs, using haemoglobin as an antigen/template model. The affinity of the produced nanoMIPs was found by both techniques to match that of high affinity monoclonal antibodies (K_D values in the nanomolar

range[34]). We demonstrate the impact of differences in the physical characteristics of nanoMIPs and antibodies on each technique. Importantly, EC offers a less complex, cheaper and faster method for characterizing nanoMIPs compared to SPR. Nonetheless, by directly comparing natural and synthetic counterparts, this work validates the produced nanoMIPs as appropriate alternatives for replacing polyclonal animal derived antibodies in immunodiagnostics and biological extraction with potential to also replace monoclonal antibodies.

2. Experimental

2.1. Materials

N-Hydroxymethylacrylamide (NHMA, 48% w/v), *N*,*N*′-methylenebisacrylamide (MBAm), ethylene glycol, iron chloride ($FeCl_3{\cdot}6H_2O$), methylhydroquinone (MHQ), sodium acetate (NaOAc), phosphate buffered saline tablets (PBS, 10 mM, pH 7.4 ± 0.2), potassium ferricyanide ($K_3Fe(CN)_6$), potassium chloride (KCl), sodium nitrate ($NaNO_3$), ammonium persulphate (APS), potassium peroxydisulfate (KPS), sodium dodecyl sulphate (SDS), 1-ethyl-3-(3-dimethylaminopropyl) carbodiimide (EDC), *N*-hydroxysuccinimide (NHS), acetic acid (AcOH), bovine haemoglobin (BHb), bovine serum albumin (BSA), Tween® 20 and glutaraldehyde (25% v/v) were used as received from Merck. Haemoglobin polyclonal antibody (Hb pAb) was purchased from Invitrogen (Thermo Fisher Scientific, UK). Buffers were prepared in Milli-Q water (resistivity 18.2 ± 0.2 MΩ cm). DropSens disposable screen-printed electrodes (Au-BT) comprising a gold working electrode (0.4 cm diameter), a platinum counter electrode and a silver reference electrode were purchased from Metrohm (Runcorn, Cheshire, UK). Carboxymethyl dextran hydrogel gold sensor slides were purchased from ATG Scientific Ltd (Oxford, UK).

2.2. Instrumentation

An Anton Paar Monowave 200 microwave oven for MNP synthesis was purchased from Anton Paar Ltd, Hertfordshire, UK. An SLS Lab Basics centrifuge (Scientific Laboratory Supplies, Nottingham, UK) was used to separate MNP/nanoMIPs from supernatants. A Zetasizer Ultra (Malvern PANalytical, Worcestershire, United Kingdom) was used to determine the nanoMIP particle hydrodynamic diameter and particle concentration. A Reichert 2 SPR system (Reichert Technologies, Buffalo, USA) and TraceDrawer software were used for kinetic analysis.

2.3. MNP production

Bare and aldehyde functionalised magnetic particles were produced following our previously published solvothermal microwave method.[35–37] Briefly, 0.5 g of $FeCl_3{\cdot}6H_2O$ and 1.8 g of NaOAc were dissolved in 15 mL of ethylene glycol in a 30 mL Anton Parr G30 microwave reaction vial (MRV). Glutaraldehyde (3.5 mL) was then added to the resulting solution with stirring for a further 5 min. The stirrer bar was then removed and the MRV was placed in an Anton Paar Monowave 200 microwave oven and the reaction mixture was heated up to a temperature of 200 °C with a ramp time of 18 °C min^{-1} (over 10 min). The reaction was held at 200 °C for 20 min under pressure (9 bar). The resulting composite products were allowed to cool for 10 min, washed five times with deionised water, followed by two washes of ethanol, and then isolated with a neodymium magnet and then resuspended in deionised water and stored at 4 °C.

2.4. BHb functionalization of MNPs

A suspension (1 mL) equivalent to 0.010 g of the produced aldehyde functionalised magnetic nanoparticle (MNP@CHO) was placed in an Eppendorf microcentrifuge tube. A neodymium magnet was placed on the side of the tube to rapidly pull the magnetic nanoparticles from the solution (10 minutes). The supernatant was removed and replaced with 1 mL of 1 mg mL^{-1} lyophilised BHb in PBS. The Eppendorf tube was then sonicated for 2 minutes followed by vigorous shaking and vortexing to ensure that the nanoparticles were fully dispersed. The reaction mixture was left undisturbed at room temperature (22 °C) for 30 minutes, allowing the protein to conjugate with MNP@CHO. After 30 minutes, the particles were once again separated from the solution and the supernatant was exchanged with fresh buffer in triplicate to remove any non-conjugated protein. The resulting MNP@CHO@BHb particles thus produced were stored wet at 4 °C until further use.

2.5. NanoMIP production using MNP@CHO@BHb

With sonication followed by vigorous shaking and vortex mixing, the magnetic nanoparticles (0.011 g) were resuspended in 906 μL of PBS (pH7.4) and transferred to a 15 mL Falcon tube. The tube was then placed in a thermo-mixer and set to mix at 400 rpm at room temperature. The sample was then degassed using nitrogen for 15 minutes with stirring. The nitrogen line was then removed and 37 mg of NHMA monomer (77 μL of 48% v/v solution) and 6 mg of MBAm were immediately added to the reaction mixture, followed by 40 μL of a solution containing 10% (v/v) TEMED and 5% (w/v) APS. A nitrogen headspace was then created, and the Falcon tube was sealed with the cap and then wrapped in parafilm. The solution was allowed to mix at 400 rpm for 15 minutes to allow nanoMIP particles to be produced at the surface of the MNP@CHO@BHb particles.

At 15 minutes, the reaction was rapidly quenched with 1 mL of 10 mM MHQ. The reaction solution was exchanged three times with fresh PBS to remove any unreacted monomers and quencher. The solution was then resealed, and the tube was placed on its side on a neodymium magnet (2 minutes). The supernatant was then removed. The MNP@CHO@BHb ~ nanoMIP particles were dispersed in 600 μL of e-pure water and placed in a VWR® ultrasonicator (600 W, 45 kHz) for 5 minutes at 37 °C. The Falcon tube was then once again placed on a neodymium magnet and the supernatant now containing the released nanoMIPs was placed in a 1 mL volume Eppendorf and lyophilized at −76.3 °C and 0.0010 mbar using a CHRIST Alpha 2-4 LSCbasic freeze-dryer.

2.6. Physical characterization of nanoMIPs and antibodies by dynamic light scattering (DLS) and nanoparticle tracking analysis (NTA)

The hydrodynamic diameter and particle concentration of NanoMIPs were determined by DLS and multi angle dynamic light scattering (MADLS) using a Zetasizer Ultra and confirmed using NanoSight Pro (version 1.1) NTA. Lyophilized NanoMIPs were resuspended in PBS, and measurements were performed in triplicate using a disposable cuvette (refractive index 1.32). For NTA analysis, nanoMIPs were resuspended and diluted 50 times in particle free PBS. A low volume flow cell (LVFC) was mounted onto a 488 nm laser module and light scattering was recorded using a highly sensitive sCMOS camera. 5 captures (750 frames) were recorded for each measurement. The samples were equilibrated for 60 s prior to measurement. The size and concentration of Hb pAbs were assessed by DLS and MADLS, respectively, in a similar way to that for nanoMIPs.

2.7. Integration of nanoMIPs and antibodies into an electrochemical sensor

All electrochemical experiments were performed using a Metrohm Autolab PGSTAT204 pontentiostat and NOVA2.1.6 software. NanoMIPs were eluted using sonication and were then entrapped within an electropolymerized layer (E-layer). E-layers were fabricated directly onto BT-Au screen-printed electrodes (SPEs; Metrohm) using cyclic voltammetry (CV) largely following the procedure in ref. 38. Briefly, a 50 μL solution in PBS comprising 0.1 mg of nanoMIPs, 641 mM NHMA as the functional monomer, 41.5 mM MBAm as the cross-linker, 0.29 M $NaNO_3$, and 48.15 mM KPS was deposited onto the SPE. The potential was then cycled between −0.2 V and −1.4 V for 7 cycles at 50 mV s^{-1} (10 min, RT, 22 ± 2 °C) to produce the E-layer with entrapped nanoMIPs. Haemoglobin polyclonal antibodies were entrapped in the E-layer in the same fashion, using 0.1 μg from a 0.5 mg mL^{-1} solution instead of nanoMIPs. E-layers in the absence of nanoMIPs or antibodies were also produced as a control.

2.8. Electrochemical studies of nanoMIPs and antibodies

The E-layer comprising entrapped nanoMIP islands (E-NMI) or entrapped Hb pAb was exposed to varying concentrations of target protein (BHb) template solutions over a wide concentration range (100 fM to 100 μM) for a period of 5 minutes at each concentration.

Selective protein binding was tracked using either cyclic voltammetry or electrochemical impedance spectroscopy (EIS) of an external 5 mM potassium ferricyanide solution in PBS containing 0.5 M KCl as a supporting electrolyte. Electrochemical impedance spectroscopy (EIS) measurements were conducted at a standard potential of 0.1 V (±0.01 V) with 10 scans of frequencies, and a sinusoidal potential peak-to-peak with an amplitude of 0.01 V in the frequency range of 0.1–100 000 Hz. A Randles equivalent circuit was fitted for all EIS experiments using the FRA32 module.[9]

2.9. Surface plasmon resonance studies

Using a Reichert 2SPR system (Reichert Technologies, Buffalo, USA), experiments were performed using an adapted methodology to provide accurate binding affinities of the imprinted materials. Carboxymethyl dextran hydrogel coated Au chips were installed as per the manufacturer's instructions. Running buffer PBST (PBS pH 7.4 and 0.01% Tween 20) was flowed over the sensor surface at 10 μl min^{-1} until the baseline was stable, with this flow rate of 10 μl min^{-1} being maintained throughout the immobilisation process. For the immobilisation of the nanoMIP, a fresh solution of EDC (40 mg) and NHS (10 mg) dissolved in 1 ml of water was injected onto the sensor chip surface for 6 min. This enables the activation of carboxyl groups contained within the carboxymethyl dextran layer. Next the nanoMIPs (1 mg) dissolved in 1 ml of 10 mM sodium acetate (0.82 mg ml^{-1}, pH 5.2) were injected only into the left channel of the activated surface for 10 min. To deactivate the surface, a quenching solution (1 M ethanolamine, pH 8.5) was then injected for 8 min, enabling the deactivation of the carboxyl groups. This provides a sensor surface with nanoMIPs immobilised onto the left channel as the working channel, while the right channel is used as a reference control.

Binding kinetic analysis was performed using existing methodologies[39–41] at a flow rate of 25 μl min^{-1} and initiated by injection of the running buffer PBST (blank) onto the nanoMIP immobilised sensor surface with 2 min of association, followed by 7 min of dissociation.[41,42] The binding kinetics of the individual nanoMIPs towards the analyte (BHb) was determined by the association of the analyte between 4 and 64 nM BHb in PBST. After dissociation a regeneration buffer (20 mM HCl, pH 2) was used to remove the analyte from the nanoMIPs, thus renewing the sensor surface.

Signals from the working channel (left) were subtracted from those of the respective reference channel (right), to reveal the specific binding of the nanoMIPs. The SPR responses were fitted using a 1 : 1 Langmuir bio-interaction (BI) model using TraceDrawer Software. The association rate constant (k_{on}), dissociation rate constant (k_{off}), and maximum binding (B_{max}) were fitted globally, whereas the BI signal was fitted locally. The equilibrium dissociation constant (K_D) was calculated as k_{off}/k_{on}. The experiment was repeated by replacing the BHb target protein with the BSA non-target to assess the degree of non-specific binding and nanoMIP selectivity.

In a similar method to nanoMIP immobilisation, BHb polyclonal antibodies (BHb pAbs) were immobilized on the sensor surface using a 2 μg ml^{-1} solution from a 0.5 mg mL^{-1} stock BHb pAbs solution and analysed in the same manner as immobilised nanoMIPs.

3. Results and discussion

3.1. DLS and NTA analyses of nanoMIPs and pAb

High affinity nanoMIPs for bovine haemoglobin (BHb) were prepared using a new and scalable method, resulting in 10 ± 2 mg of nanoMIPs being produced in less than 1 h.[36] The

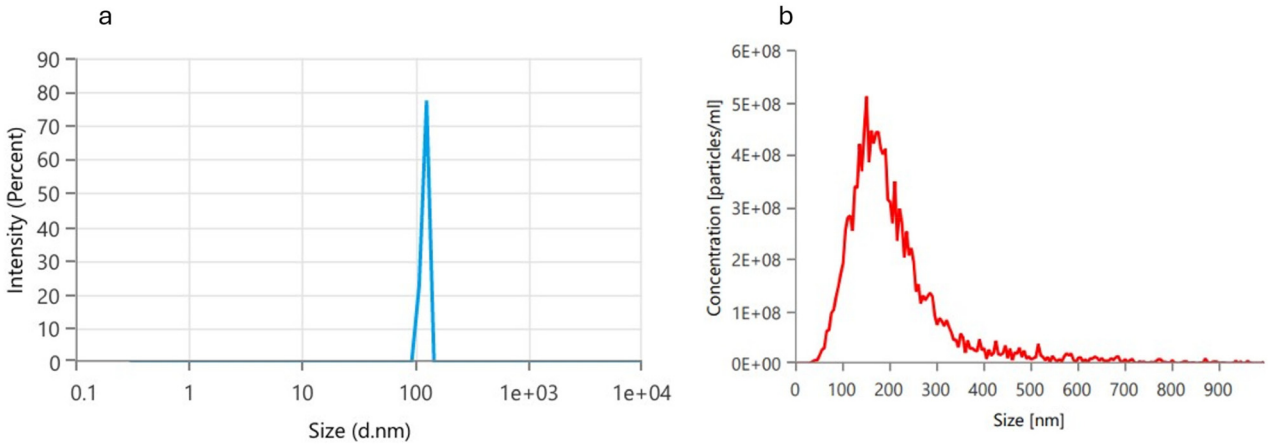

Fig. 1 Particle size analysis of BHb nanoMIPs using dynamic light scattering (DLS; a) and particle concentration analysis using nanoparticle tracking analysis (NTA; b).

nanoMIPs (1 mg mL^{-1}) were characterised using dynamic light scattering (back scatter) (Fig. 1a) and nanoparticle tracking analysis (Fig. 1b) to obtain particle hydrodynamic diameter distribution and particle concentration. It should be noted that samples needed to be diluted by a factor of 10 for DLS analysis to minimize error due to multiple scattering of aggregates. DLS showed that particles were monodisperse with a diameter of 121 ± 53 nm with a yield concentration of 2.39 × 10^{10} particles per mL, as obtained by MADLS. NTA demonstrated a particle concentration of 1.4 × 10^{10} particles per mL, demonstrating good agreement with MADLS results. The hydrodynamic diameter determined using NTA gave a value of 180 ± 15 nm with the lower standard deviation giving higher confidence in size measurement.

The observed differences in standard deviation can be attributed to the distinct modes of operation employed by NTA and DLS. In NTA, samples are analysed using a flow-based system in which individual particles pass through a detection cell, where they are imaged, tracked, and measured on a particle-by-particle basis. This approach provides a more accurate assessment of particle size distributions, as it minimizes aggregation and is particularly well-suited for polydisperse samples. In contrast, DLS measurements are performed under quiescent conditions, where particles remain stationary during analysis. Under these conditions, particle aggregation and sedimentation are more likely to occur, resulting in the measurement of ensemble-averaged scattering signals. Consequently, the apparent particle size often increases over the course of the measurement, leading to greater variability and a larger standard deviation compared with NTA.

The DLS spectrum (see SI Fig. S1) for the bovine haemoglobin polyclonal antibody (BHb pAb) shows a monodisperse particle distribution with a hydrodynamic average diameter of 87 ± 20 nm. The average hydrodynamic size of antibodies typically ranges from 9 to 12 nm,[30] and thus possibly the result is representative of antibody aggregates, which tend to happen when in solution. The particle concentration obtained by MADLS was found to be 4.28 × 10^{10} particles per mL, similar to the concentration found for the nanoMIPs.

3.2. SPR analysis of BHb pAb *vs.* BHb nanoMIP

By virtue of the solid-phase imprinting process, the binding cavities formed in nanoMIPs inherently represent a heterogeneous population of recognition sites. These sites can arise from interactions with different regions and conformations of the target protein during synthesis. As such, the binding sites of the nanoMIPs are more analogous to those of a polyclonal antibody, which similarly recognises multiple epitopes of the same antigen. Although the affinity of individual nanoMIP binding sites can approach that of monoclonal antibodies, the collective nature of the nanoMIP binding sites more closely mirrors the multi-epitope variable regions of polyclonal antibodies. Fig. 2 shows the surface plasmon resonance sensorgrams for association (k_{on}) and dissociation (k_{off}) of BHb to an SPR chip pre-modified with either a BHb nanoMIP (Fig. 2a) or a BHb pAb (Fig. 2b), respectively. The unfitted data for Fig. 2a are shown as an example in SI Fig. S2 before blank subtraction for each concentration studied. As can be seen, each raw dataset closely follows what is shown in the fitted data and therefore should be considered a very good fit. Subsequent to association, we see that there is slow dissociation of protein from nanoMIPs compared with the relative ease of protein unbinding (fast dissociation) from pAb. This in turn is reflected in the corresponding equilibrium binding constants ($K_D = k_{off}/k_{on}$) determined for each, giving a K_D value of 3.06 pM for the BHb nanoMIP, a value more typical of a monoclonal antibody (mAb), and a value of 48.7 nM for the BHb pAb, a value typical of a polyclonal antibody.[43] This confirms the high affinity of the nanoMIPs for the target protein. The calculated k_{on} and k_{off} rates for both the nanoMIP and antibody are shown in SI Table S1.

Fig. 3a and b show the SPR responses of binding a non-target protein, bovine serum albumin (BSA), to the BHb nanoMIP and BHb pAb, respectively. The SPR sensorgram for

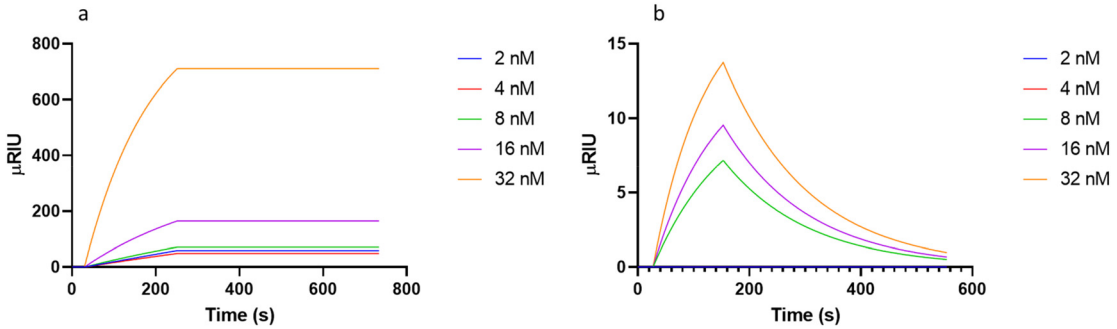

Fig. 2 Surface plasmon resonance (SPR) sensorgrams for target BHb protein binding to SPR chips modified with BHb NanoMIPs (a) and BHb pAbs (b) with the two lowest concentrations shown as a singular blue line demonstrating no notable response.

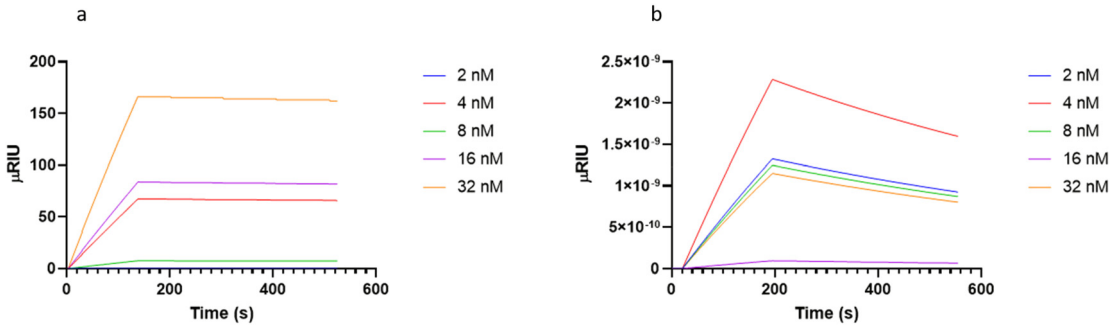

Fig. 3 Surface plasmon resonance (SPR) sensorgrams for non-target BSA protein binding to SPR chips modified with BHb nanoMIPs (a) and BHb pAbs (b).

the BHb nanoMIP with non-target BSA demonstrates an affinity profile with rapid association and slow dissociation kinetics but the dissociation with the non-target is notably faster than it is for the target BHb (Fig. 2a). The generated signals for the non-target binding are, on average, 4× smaller than those for the target binding to the nanoMIP. The SPR sensorgram for the binding interactions of five concentrations of non-target BSA to the immobilized Hb pAb shows slower association and dissociation compared to the target, which could be attributed to the sticky nature and some non-specific binding of BSA.[44] However, the changes in the refractive index are significantly smaller for the non-target, indicating the high selectivity of Hb pAb to BHb over BSA and lower affinity.

3.3. Electrochemical impedance spectroscopy analysis of the BHb pAb *vs.* BHb nanoMIP

EIS analysis is demonstrated to be a valuable technique in analysing small concentration changes and binding characteristics of polymer adlayers on an electrochemical electrode. The nanoMIPs were physically entrapped within an electrochemically grown hydrogel film using a previously reported method.[6] The nanoMIPs are present on the surface as a homogeneous distribution,[9] making them ideal for subsequent protein binding analysis using EIS when the electrode is investigated with a fixed concentration of a model redox marker such as ferrocyanide. Using the Randles model circuit,[7,36,38,45] we could determine the change in charge transfer resistance (R_{CT}), which serves as a useful indicator of the extent of target and non-target protein binding to nanoMIP particles.

Fig. 4 shows the R_{CT} values obtained for target protein (BHb) and non-target (BSA) binding to the BHb nanoMIP (4a and 4b) and pAbs (4c and 4d) modified electrodes. For the target, data from three independent electrodes were averaged across a wide concentration range (10^{-13} to 10^{-8} M). The data from target binding to the BHb nanoMIP (Fig. 4a) show that there is no detectable response at 100 fM, followed by a linear response between 1 pM and 100 nM (R^2 = 0.927; see SI Fig. S3 for the regression line), and reaching saturation at 1 μM. The BHb nanoMIP sensor exhibits changes ranging from 10 to several hundred ohms within this concentration range. The results indicate proportional changes in charge transfer resistance (R_{CT}) with target protein binding. Using the Hill–Langmuir equation we determined K_D to be 34.7 pM ± 2 pM, which is in good agreement with the SPR analysis.

The differing levels of non-specific binding observed for nanoMIPs and pAbs across SPR and EIS stem primarily from the degree to which each platform is inherently optimised for the respective recognition elements. SPR instruments and their associated surface chemistries (*e.g.* EDC-NHS immobilisation and ethanolamine passivation of the unused surface) are

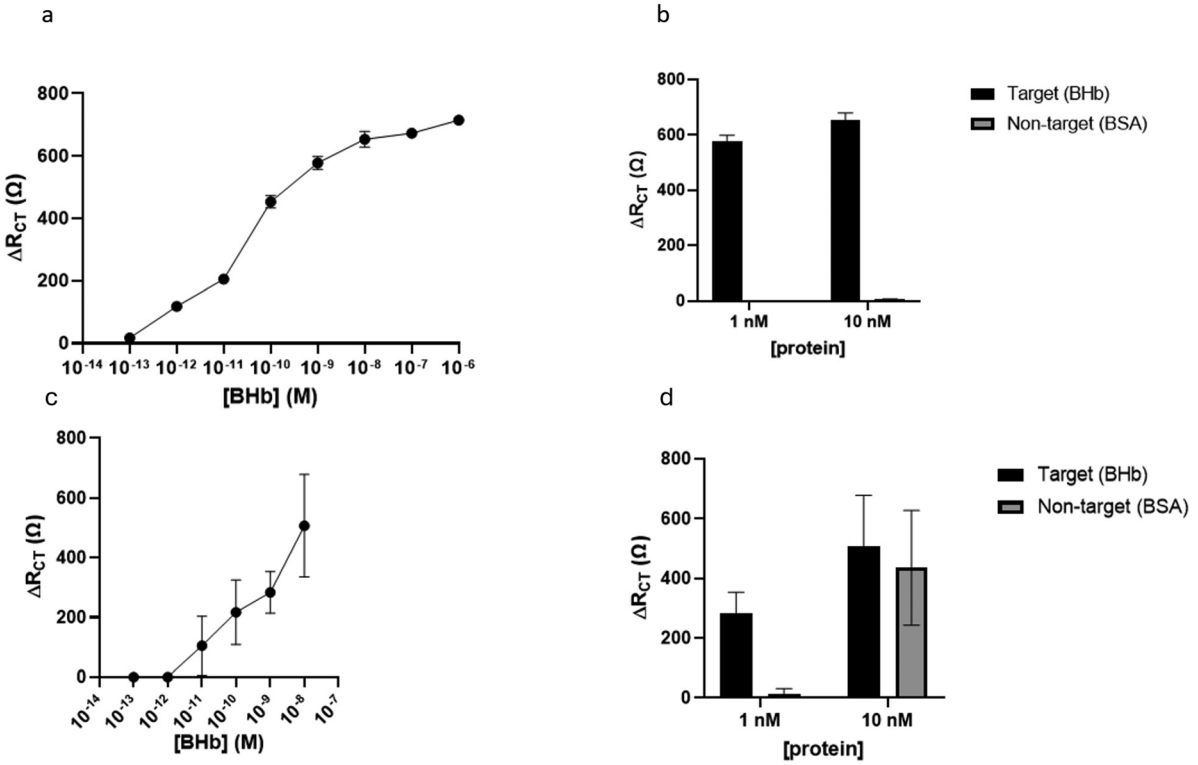

Fig. 4 Comparison of R_{CT} values obtained of target (BHb; a) and non-target (BSA; b) protein binding respectively to the BHb nanoMIP modified electrode. Comparison of the R_{CT} values obtained for target (BHb; c) and non-target (BSA; d) protein binding respectively to the Hb pAb modified electrode over a similar range of protein concentrations. Data represent mean ± S.E.M., n = 3.

highly optimised for protein-based assays, particularly antibodies. The immobilisation and assay conditions used here therefore favour pAbs, resulting in negligible non-specific binding in the SPR format. In contrast, the same conditions are not highly tailored for nanoMIPs, leading to higher apparent non-specific binding observed for the nanoMIP under SPR. With the nanoMIP particles having sizes ranging from 100 to 120 nm, they are a factor of 10 larger than the corresponding antibody, which could lead to less dense packing of the affinity reagent at the SPR surface. Additionally, there is no control of the orientation of these nanoMIP particles, which could lead to non-uniform packing and distribution of nanoMIPs on the SPR surface compared with the corresponding antibody. However, there is good agreement of K_D values between EIS and SPR for nanoMIPs, suggesting that there is an equivalence in the binding capacity of surface immobilised nanoMIPs on both electrochemical electrode and SPR chip surfaces.

Conversely, the EIS platform used in this study has been specifically optimised for nanoMIP-based sensing. In our system, the nanoMIPs are uniformly entrapped within an electrochemically grown polymer thin film formed directly on the electrode surface, creating a stable and selective environment that suppresses non-specific binding.[36] In a recent study using AFM imaging, nanoMIPs were found to be uniformly distributed and present as protruding islands in a sea of electrochemically grown surface fixing polymers. Under these optimised conditions, nanoMIPs exhibit excellent specificity. In contrast, pAbs being less than $1/10^{th}$ of the size of nanoMIPs are likely being buried within the growing polymeric surface and therefore a large proportion becomes inaccessible for affinity binding to the target, which potentially leads to higher levels of non-specific binding with pAbs on an electrochemical system. The lack of agreement in K_D for pAbs between SPR and electrochemical determinations likely suggests that only a small concentration of antibody binding sites is available with the electrochemical system (due to most antibodies being immersed within the polymer thin film layer and therefore inaccessible) compared to the chemically immobilised antibody on the SPR system.

In contrast when the non-target protein BSA (at 1 nM and 10 nM) is analysed on the BHb nanoMIP sensor (Fig. 4b), there is no significant change in R_{CT}, with a signal of only 5 Ω at 10 nM, indicating that non-specific binding is negligible. This is further supported by previous studies where the nanoMIP specificity was tested in foetal calf serum inherently comprising albumin, which could potentially interfere with target protein detection.[9] Selectivity here was retained after a simple 1 : 10 dilution of the serum. No dilution of the sample was required to minimise interference from synthetic urine.[27]

Fig. 4c and d show a comparison of the change in R_{CT} obtained following target protein (BHb) and non-target (BSA)

binding, respectively, to the Hb pAb modified electrode over a similar range of protein concentrations. Interestingly, the concentration profile demonstrates a saturation phase (steady-state signal) between 10^{-10} M and 10^{-9} M, followed by a subsequent increase in R_{CT} at a higher protein loading (see SI Fig. S4). We understand the saturation to be due to homogeneous (1 : 1) binding of the target protein to the pAb. However, with an increase in target concentration we observe a heterogenous binding phase due to the occurrence of significant protein–protein interaction. This effect was recently reported by Sherer and Cho[46] in their biolayer interferometry studies of protein (TRIM25) to receptor (NS1) binding interactions.

The K_D for Hb pAb was subsequently determined using the Hill–Langmuir equation to be 51.9 ± 0.7 pM, demonstrating higher selectivity compared with SPR results. The difference could be attributed to more antibodies being electrochemically entrapped in a polymeric layer per unit area than are chemically immobilized (using EDC/NHS coupling) on the SPR sensor chip. In addition, the small size of the pAb could also contribute to an increased antibody concentration on the polymeric E-layer.

Table 1 provides a summary of affinity constants and protein target molecules for antibodies or nanoMIPs that were studied in isolation. We include the results for our combined study of pAb *vs.* nanoMIPs. The comparison demonstrates that the method presented in this study yields binding affinities consistent with those obtained using established antibody standard characterization techniques such as biolayer interferometry (BLI), confirming the validity and reliability of our SPR and electrochemical approaches.

Table 2 shows a direct comparison of nanoMIPs and polyclonal antibodies for BHb including the relative size of each of the particles, their concentration as used to make layers on either the electrochemical electrode or the SPR chip surface and the subsequent impact on the equilibrium dissociation constant (K_D) and selectivity factor (SF) when tested against the non-target protein BSA. It should be noted that the selectivity factor was calculated using EIS data by taking the signal ratio of target : non-target at 10 nM.

The electrochemical method works in the static mode, meaning that the analyte samples are introduced to the sensor for a fixed period as a droplet before being removed and the sensor is rinsed to remove the non-specifically bound analyte. Then any specific binding is determined using EIS. We subsequently add further analytes at increasing fixed concentrations in the same fashion until EIS signal saturation is reached. There is clearly a strong linear dependence between the concentration and EIS signals (over a wide dynamic concentration range), as seen in Fig. 4a and SI Fig. S3, allowing us to use signals at a particular concentration of the analyte (*e.g.* 1 nM or 10 nM) for target : non-target selectivity determination.

In contrast to the EIS approach, SPR is a kinetic, flow-based technique that enables direct determination of both association ("on", binding) and dissociation ("off", unbinding) rates.

Table 1 Summary of detection techniques, affinity constants, and target molecules for antibodies or nanoMIPs studied in isolation compared with our Ab *vs.* nanoMIP combined study

Detection techniques	Affinity reagent	Average K_D	Target	Ref.
Bio-layer interferometry (BLI) and titration kinetic (TK) assays	mAb	10^{-8}–10^{-10} M (BLI) 10^{-8}–10^{-10} M (TK)	A range of proteins (21–145 kDa)	47
Bio-layer interferometry (BLI)	Manose nanoMIP	10^{-10} M	Wild-type SARS-CoV-2 pseudovirus	48
Fluorescence-activated cell sorting (FACS), flow cytometry, and kinetic exclusion assay	mAb	10^{-10} M (FACS) 10^{-11} M (kinetic exclusion assay)	CD 20	49
Piezoelectric quartz crystal	mAb	3.21×10^{-10} M	Alpha fetoprotein (AFP)	50
Piezoelectric quartz crystal	MIP thin film	3.17×10^{-9}M	Glycoprotein 41	51
EIS	mAb	5.3×10^{-11} M	p-Tau181	52
EIS	NanoMIP	3.74×10^{-11} M	Bovine haemoglobin	6
SPR	mAb	9.0×10^{-10} M	β2-Microglobulin	53
SPR	pAb	4.87×10^{-8} M	Bovine haemoglobin	This paper
SPR	NanoMIP	3.06×10^{-12} M	Bovine haemoglobin	This paper

Table 2 Summary of physical (size and particle concentration) and binding affinity characterization and selectivity factor (SF) determination for nanoMIP and antibody

Affinity reagent	Size (nm)	Particle concentration (particles per mL)	K_D (EIS)	K_D (SPR)	SF (EIS) Based on target : non-target signal at 10 nM
nanoMIP	121	2.39×10^{10}	34.7 pM	3.06 pM	130 : 1
pAb	86.94	4.28×10^{10}	51.9 pM	48.7 nM	1.0 : 1.1

However, SPR exhibits lower sensitivity at low target concentrations compared with EIS. As a result, assessing the selectivity factor based solely on raw association data can introduce substantial error. SPR was therefore used as a method to directly compare K_D values of antibodies to nanoMIPs and not intended as a biosensor for accurate analyte detection.

The difference of several orders of magnitude in the apparent K_D values for the pAb obtained by SPR *versus* EIS (Table 2) arises from fundamental differences in how the antibody is immobilised on each platform. SPR provides highly controlled antibody immobilisation and preserves access to the antigen-binding regions. In contrast, the EIS sensing surface used in this work involves entrapment of the recognition elements within a polymer thin film. For antibodies, this lack of control over molecular orientation means that a portion of the binding sites is likely to be partially or fully occluded by the polymer layer. Because the thickness of the film can approach the dimensions of an IgG (~10–15 nm), the effective number of antibody binding sites available for analyte interaction is reduced compared to SPR, where no such overlay exists. An additional consideration with the electrochemical method is that the crosslinking density of the immobilising polymer film is insufficient to immobilise the polyclonal antibody. The pAb could therefore have leached out of the thin film, leaving a highly nanoporous, thin film layer, thus allowing subsequent non-specific binding of both target and non-target proteins alike and resulting in poor selectivities for the electrochemical pAb system.

This reduced accessible binding capacity, caused by either a very low concentration of antibody binding sites present on the surface of the entrapping polymer layer or antibodies being lost by leaching, presents two important consequences for the extracted K_D when fitting EIS data using the Hill–Langmuir model. First, because the antibody saturates at a lower apparent surface occupancy, the fitted maximum signal (B_{max}) is underestimated. Second, since the EIS-based calculation relies on the relationship $K_D = \frac{1}{2}B_{max}$, an underestimated B_{max} artificially lowers the calculated K_D, giving the appearance of an unrealistically high affinity. This effect is much more pronounced for antibodies than for the nanoMIPs: the MIPs are ~120 nm in size, contain multiple binding sites per particle, and are therefore far less affected by partial surface occlusion within the thin film.

These observations indicate that while the Langmuir model is appropriate for the nanoMIP data under EIS conditions, it is not fully suitable for the antibody data, given the reduced binding-site accessibility and lack of optimisation of the electrochemical platform for pAb immobilisation. The discrepancy could be mitigated by further optimisation such as reducing the film thickness through cycle-level optimisation of the CV deposition step and/or increasing the crosslinking density of the thin film.

4. Conclusions

We have demonstrated, for the first time, a direct comparison of binding affinities of a biologically sourced polyclonal antibody (pAb) *versus* synthetic nanoscale molecularly imprinted polymer (nanoMIP) for a common protein target, bovine haemoglobin (BHb). We used two analytical methods of determining equilibrium dissociation constants (K_D) and selectivity. Our results show that nanoMIPs display higher monoclonal-like affinity to the target protein compared with pAb. Additionally, whereas the response to the non-target protein (BSA) is negligible for the BHb nanoMIP, there is some cross-selectivity displayed by the Hb pAb using our electrochemical approach. Our nanoMIP technology is generic and can be applied to a range of protein targets. The nanoMIPs can be produced at low cost and at scale and speed. In addition to being an animal-friendly affinity reagent, nanoMIPs offer a realistic and commercially viable alternative to antibodies in diagnostic and biopurifcation applications.

Author contributions

S. M. R.: conceptualization, formal analysis, funding acquisition, investigation, methodology, project administration, supervision, and writing – original draft. A. N. S.: conceptualization, data curation, formal analysis, investigation, methodology, and writing – original draft. B. V. B.: data curation, formal analysis, investigation, methodology, and writing – original draft. All authors contributed to manuscript revision, and read and approved the submitted version.

Conflicts of interest

The authors declare that the research was conducted in the absence of any commercial or financial relationships that could be construed as a potential conflict of interest.

Data availability

All data are available within the article and its supplementary information (SI).

Acknowledgements

The authors are grateful to the University of Lancashire for DTC studentship funding for B. V. B., the Royal Society of Chemistry COVID-19 Action fund (H20-188) and the RSC Research Enablement Grant (E22-5899202825), the Daiwa Anglo-Japanese Foundation (13094/13916) and the Royal Society (IES\R3\193093) for funding this work. We wish to thank Dr Nellie Lalani (Malvern PANalytical) for the NTA data acquisition service and useful discussions.

References

1 P. J. Kennedy, C. Oliveira, P. L. Granja and B. Sarmento, *Crit. Rev. Biotechnol.*, 2018, **38**, 394–408.
2 C. Chen, Z. Garcia, D. Chen, H. Liu and P. Trelstad, *mAbs*, 2025, **17**, 2451789.
3 A. C. Gray, A. R. M. Bradbury, A. Knappik, A. Plückthun, C. A. K. Borrebaeck and S. Dübel, *Nat. Methods*, 2020, **17**, 755–756.
4 J. Barroso, M. Halder and M. Whelan, *EURL ECVAM recommendation on non-animal-derived antibodies*, Publications Office of the European Union, 2020.
5 A. Gray, Ac Fau-Bradbury, S. Bradbury, A. Fau-Dübel, A. Dübel, S. Fau-Knappik, A. Knappik, A. Fau-Plückthun, C. A. K. Plückthun, A. Fau-Borrebaeck and C. A. K. Borrebaeck.
6 S. M. Reddy, A. N. Stephen, M. A. Holden, W. J. Stockburn and S. R. Dennison, *Biomater. Sci.*, 2024, **12**, 5845–5855.
7 A. N. Stephen, M. A. Holden, M. V. Sullivan, N. W. Turner, S. R. Dennison and S. M. Reddy, *Biomed. Mater.*, 2025, **20**, 025043.
8 O. I. Parisi, F. Francomano, M. Dattilo, F. Patitucci, S. Prete, F. Amone and F. Puoci, *J. Funct. Biomater.*, 2022, **13**, 12.
9 A. N. Stephen, S. R. Dennison, M. A. Holden and S. M. Reddy, *Analyst*, 2023, **148**, 5476–5485.
10 H. F. El Sharif, S. R. Dennison, M. Tully, S. Crossley, W. Mwangi, D. Bailey, S. P. Graham and S. M. Reddy, *Anal. Chim. Acta*, 2022, **1206**, 339777.
11 M. V. Sullivan, S. R. Dennison, G. Archontis, S. M. Reddy and J. M. Hayes, *J. Phys. Chem. B*, 2019, **123**, 5432–5443.
12 H. F. El-Sharif, N. W. Turner, S. M. Reddy and M. V. Sullivan, *Talanta*, 2022, **240**, 123158.
13 H. F. El-Sharif, H. Yapati, S. Kalluru and S. M. Reddy, *Acta Biomater.*, 2015, **28**, 121–127.
14 H. F. El-Sharif, D. M. Hawkins, D. Stevenson and S. M. Reddy, *Phys. Chem. Chem. Phys.*, 2014, **16**, 15483–15489.
15 F. Canfarotta, A. Poma, A. Guerreiro and S. Piletsky, *Nat. Protoc.*, 2016, **11**, 443–455.
16 X. Shen, C. Huang, S. Shinde, K. K. Jagadeesan, S. Ekström, E. Fritz and B. Sellergren, *ACS Appl. Mater. Interfaces*, 2016, **8**, 30484–30491.
17 N. Yucel, H. Gulen and P. C. Hatir, *J. Appl. Polym. Sci.*, 2022, **139**, e52952.
18 A. Henderson, M. V. Sullivan, R. A. Hand and N. W. Turner, *J. Mater. Chem. B*, 2022, **10**, 6792–6799.
19 H. J. Lim, T. Saha, B. T. Tey, S. K. Lal and C. W. Ooi, *Surf. Interfaces*, 2023, **39**, 102904.
20 M. Sönmezler, E. Özgür, H. Yavuz and A. Denizli, *Artif. Cells, Nanomed., Biotechnol.*, 2019, **47**, 221–227.
21 A. Raziq, A. Kidakova, R. Boroznjak, J. Reut, A. Öpik and V. Syritski, *Biosens. Bioelectron.*, 2021, **178**, 113029.
22 Y. Li, L. Luo, Y. Kong, Y. Li, Q. Wang, M. Wang, Y. Li, A. Davenport and B. Li, *Biosens. Bioelectron.*, 2024, **249**, 116018.
23 M. V. Sullivan, A. Henderson, R. A. Hand and N. W. Turner, *Anal. Bioanal. Chem.*, 2022, **414**, 3687–3696.
24 A. Abbas, M. J. Linman and Q. Cheng, *Sens. Actuators, B*, 2011, **156**, 169–175.
25 Y. Wang, Q. Zhang, Y. Ren, L. Jing and T. Wei, *Chem. Res. Chin. Univ.*, 2014, **30**, 42–48.
26 S. Akgönüllü, S. Kılıç, C. Esen and A. Denizli, *Polymers*, 2023, **15**, 629.
27 A. Stephen and S. Reddy, *Analyst*, 2025, **150**, 4293–4303.
28 T. Špringer, M. Bocková, J. Slabý, F. Sohrabi, M. Čapková and J. Homola, *Biosens. Bioelectron.*, 2025, **278**, 117308.
29 D. Capelli, V. Scognamiglio and R. Montanari, *TrAC, Trends Anal. Chem.*, 2023, **163**, 117079.
30 J. Arora, Y. Hu, R. Esfandiary, H. A. Sathish, S. M. Bishop, S. B. Joshi, C. R. Middaugh, D. B. Volkin and D. D. Weis, *mAbs*, 2016, **8**, 1561–1574.
31 S. S. Piletsky, A. E. G. Cass, E. V. Piletska, J. Czulak and S. A. Piletsky, *ChemNanoMat*, 2018, **4**, 1214–1222.
32 K. Smolinska-Kempisty, A. Guerreiro, F. Canfarotta, C. Cáceres, M. J. Whitcombe and S. Piletsky, *Sci. Rep.*, 2016, **6**, 37638.
33 A. N. Stephen, T. Mercer, W. Stockburn, S. R. Dennison, J. E. Readman and S. M. Reddy, *Mater. Adv.*, 2025, **6**, 2016–2028.
34 S. Liu, H. Zhang, J. Dai, S. Hu, I. Pino, D. J. Eichinger, H. Lyu and H. Zhu, *mAbs*, 2015, **7**, 110–119.
35 A. N. Stephen, T. Mercer, W. Stockburn, S. R. Dennison, J. E. Readman and S. M. Reddy, *Mater. Adv.*, 2025, **6**, 2016–2028.
36 S. M. Reddy, A. N. Stephen, M. A. Holden, W. J. Stockburn and S. R. Dennison, *Biomater. Sci.*, 2024, **12**, 5845–5855.
37 M. Sullivan, W. Stockburn, P. Hawes, T. Mercer and S. Reddy, *Nanotechnology*, 2020, **32**, 095502.
38 A. Stephen, S. Dennison, M. Holden and S. Reddy, *Analyst*, 2023, **148**, 5476–5485.
39 M. V. Sullivan, F. Allabush, D. Bunka, A. Tolley, P. M. Mendes, J. H. R. Tucker and N. W. Turner, *Polym. Chem.*, 2021, **12**, 4394–4405.
40 K. P. M. Geuijen, C. Oppers-Tiemissen, D. F. Egging, P. J. Simons, L. Boon, R. B. M. Schasfoort and M. H. M. Eppink, *FEBS Open Bio*, 2017, **7**, 1557–1574.
41 S. Hearty, P. Leonard and R. O'Kennedy, *Methods Mol. Biol.*, 2012, **907**, 411–442.
42 P. Gomes and D. Andreu, *J. Immunol. Methods*, 2002, **259**, 217–230.
43 O. B. Torres, A. J. Duval, A. Sulima, J. F. G. Antoline, A. E. Jacobson, K. C. Rice, C. R. Alving and G. R. Matyas.
44 Z. Zhao, M. Pan, W. Yang, C. Huang, C. Qiao, H. Yang, J. Wang, X. Wang, J. Liu and H. Zeng, *J. Colloid Interface Sci.*, 2023, **650**, 1525–1535.
45 J. E. B. Randles, *Discuss. Faraday Soc.*, 1947, **1**, 11–19.
46 N. Sherer and J.-H. Cho, *ACS Omega*, 2025, **10**, 28422–28428.
47 V. Kamat and A. Rafique, *Anal. Biochem.*, 2017, **536**, 16–31.
48 Y. Li, S. Xu, Q. Ye, H. Chi, Z. Guo, J. Chen, M. Wu, B. Fan, B. Li, C.-F. Qin and Z. Liu, *Adv. Sci.*, 2023, **10**, 2202689.
49 A. Vaish, J. S. Lin, H. J. McBride, P. J. Grandsard and Q. Chen, *Anal. Biochem.*, 2020, **609**, 113974.

50 Y. Chen and H. Shi, *Biosensors*, 2023, **13**, 917.
51 C.-H. Lu, Y. Zhang, S.-F. Tang, Z.-B. Fang, H.-H. Yang, X. Chen and G.-N. Chen, *Biosens. Bioelectron.*, 2012, **31**, 439–444.
52 M.-V. Tieu, S. H. Choi, H. T. N. Le and S. Cho, *Anal. Chim. Acta*, 2023, **1273**, 341535.
53 H. Zhao, I. I. Gorshkova, G. L. Fu and P. Schuck, *Methods*, 2013, **59**, 328–335.